ORIGINAL RESEARCH ARTICLE

Evaluation of Inter-Laminar Shear Performance of Carbon Fiber-Reinforced Composite under Quasi-Static and High-Strain-Rate Loading

Mannan Sayyad [ORCID]

As in any other composite, the interface in the carbon fiber/polymer matrix is the key factor in determining the bulk properties of the composites. Being a highly inert material, carbon fiber exhibits poor adhesion with polymer matrices. In view of this, the knowledge of inter-laminar shear properties of the interface is important. The present work aims at adapting the test methods used to characterize the inter-laminar shear behavior of carbon fiber-reinforced composite under quasi-static and high-strain-rate loading. Double-notch shear and short beam shear tests are performed on a 4.75-mm-thick carbon fiber sheet made of 8 layers to characterize inter-laminar shear strength. In the double-notch shear test, the shear strain at failure is 3.36% under quasi-static load, while for the high-strain-rate test the failure strain is 1.5%. The average inter-laminar shear strength is found to be 69.8 MPa under quasi-static load and 92.25 MPa under high-strain-rate loading. In the short beam shear test, on the other hand, the shear strain at failure is found to be 1.9% under quasi-static load, while for the high-strain-rate test the failure strain is 4.2%. The average inter-laminar shear strength of the composite layup is measured to be about 73.9 MPa and 140.7 MPa, respectively, under quasi-static and high-strain-rate loading. Overall, it is observed that failure is mostly inter-laminar and the results indicate that there is an increase in the inter-laminar shear strength from quasi-static to high strain rate.

1. Introduction

Polymer matrix composites are finding increasing use in engineering applications due to their enhanced specific properties (stiffness and strength) and increasing cost position with respect to traditional metallic alloys (Ref 1-3). Carbon fiber-reinforced composite (CFRC) is an important material used in aerospace, automotive, military equipment and many other fields due to its enhanced mechanical performance. Typically, the performance is governed by the carbon fiber, the polymer matrix and the interface: the interaction between fiber and matrix at the interface being the key parameter. Usually the failure of CFRC occurs at the interface first (Ref 4-6). For improved mechanical performance, CFRC should possess a good interface so that the load transfer between fiber and matrix occurs successfully, thereby reducing the chances of interfacial failure (Ref 7, 8).

Chee et al. (Ref 9) have studied the influence of environmental effects on various properties of bamboo/kenaf (B/K) fiber-reinforced epoxy hybrid composites. The properties included oxidation stability, complex modulus, color, thermal stability, etc. It was observed that a fair balance in the properties was obtained in the hybrid composite formulation B:K::50:50. In another study, investigation into the material's stiffness and strength was assessed in carbon fiber-reinforced polymer laminates after an impact event (Ref 10). A suitable damage model was also proposed for providing preliminary knowledge on the extent and type of damages.

Recently, Suriani et al. (Ref 11) have worked on the understanding of adhesion in natural fiber matrix by having a better control on processing methods and fiber compatibility. Moreover, an insightful work is presented in view of mechanical and structural failure of natural fiber composites (Ref 12). As far as aerospace applications are concerned, Balasubramanian et al. (Ref 13) have elaborated on the manufacturing techniques of suitable composites and Mustapha et al. (Ref 14) have presented the findings on the structural health monitoring for aerospace composite structures.

When CFRC is subjected to excessive loads, inter-laminar fracture toughness plays an essential role in the failure. In the case of bamboo as a natural polymeric composite, Sayyad et al. (Ref 15) have shown that the asymmetric distribution of inter-laminar fracture toughness is a smart strategy for avoiding premature failure under excessive bending loads. This feature can be mimicked in synthetic composites, but it needs a lot of sophistication. Hence, it is not feasible to incorporate the asymmetric toughness in routine manufacturing processes. However, the enhancement of mechanical performance of polymeric composites can be controlled by ensuring proper interface with fair ease. As the interfacial properties of a fiber-

Mannan Sayyad, Department of Mechanical Engineering, AISSMS's College of Engineering, Pune, Maharashtra 411001, India. Contact e-mail: sayyadmannan@gmail.com.

reinforced composite are of utmost importance, it is interesting to understand the shear behavior of these materials to support the design and analysis of components used in applications that involve impact and other high-strain-rate events.

Typically, there are four characteristic strengths that define the efficacy and suitability of a polymeric composite. These tests are inter-laminar tensile strength, in-plane compression strength, inter-laminar shear strength (ILSS) and adhesive bond strength. The inter-laminar tensile strength of the polymeric composites is tested using the button tension test and flexural test. The controlling parameter in the button test is the displacement rate (the relative velocity between the two ends of the specimen), whereas in the flexural tests, the controlling parameter will be the load point displacement rate (ASTM D6415). The effect of strain rate on the in-plane compressive strength is studied using rectangular specimens with the engineering strain rate as a controlling parameter (ASTM D3410). The peel strength and shear strength of the adhesive joint between metal and composite substrates is studied using configurations such as butt joints and single lap joints, the appropriate modifications. The controlling parameter in these tests is the loading rate (ASTM D3528).

Ma et al. (Ref 16) have studied the ILSS of CFRC with different interface structures and showed that the strength increases by enhancing the interaction between fiber and matrix. In another study, Zhang and Mason (Ref 17) have investigated the effect of contaminations on the overall ILSS and observed that the properties are significantly influenced by the environmental factors like water, acids, etc. Uvarov and Chudinov (Ref 18) have studied dynamic and quasi-static ILSS strength under biaxial loading conditions and found that the material is strain rate-sensitive. However, the behavior is the same at the high strain rates.

As mentioned above, for the assessment of the reliable estimates of CFRC the knowledge of interface properties is very important. The scientific interest of the present work is to determine the adhesion in the interface in quasi-static and high-strain-rate loads. In the present work, inter-laminar shear performance of CFRC is assessed in quasi-static and high-strain-rate loads using the double-notch shear (DNS) and short beam shear (SBS) tests. The controlling parameter in the double-notch test is the displacement rate (the relative velocity between the two ends of the specimen) and that in the SBS test is the load point displacement rate.

Overall in the present study, an attempt is made to evaluate the inter-laminar shear properties of carbon fiber/polymer under quasi-static and high-strain-rate loading to hypothesize the influence of loading rate on the interface properties.

2. Materials and Methods

The specimens were prepared from the composite layup of 4.75 mm thickness made of 8 layers of continuous CFRC filaments provided by GE Global Research to perform ILSS tests under quasi-static and high-strain-rate loads. For this, two sets of specimens, namely double-notch shear (DNS) and short beam shear (SBS), were prepared as mentioned in ASTM D3846 and ASTM D2344, respectively. All quasi-static tests were conducted on a universal testing machine (UTM) at a crosshead rate of 0.5 mm/minute. As mentioned earlier, the controlling parameter in the DNS test was the displacement rate

(the relative velocity between the two ends of the sample) and that in the SBS test was the load point displacement rate.

For DNS test, ASTM D 3846 suggests the use of a loading jig to prevent flexure of the ends during loading. The loading jig consisted of two parallel plates with four through holes in one and four tapped holes (of M3 size) in the other one. The two plates were placed on either side of the specimen so that the plate spans over the two notches. The jig was assembled with four fasteners. During the test, the nuts were only sung tightened to avoid exerting compressive forces on the specimen. After some initial trials, the geometry described in Fig. 1(b) was finalized for specimens and loading jig. A detailed information about the DNS and SBS specimens used in this work is shown in Fig. 1.

A random speckle pattern was applied on the specimen surface to enable displacement and strain measurements using digital image correlation (DIC). The images were captured using a 2-megapixel resolution charged-coupled device (CCD) camera at 500-millisecond intervals. The load was also recorded simultaneously by the imaging software. A SIM02-16 ultra-high-speed camera was used to capture the images of the specimen during the test. The images were captured at intervals of 10 microseconds. From the images, the displacement and strains were obtained using DIC. The un-deformed and deformed images were correlated using the Vic2D software (Correlated Solutions Inc., USA) to obtain the displacement and the strains. The experiments mentioned in this work are carried out in the High Speed Experimental Mechanics Laboratory at IIT Kanpur.

3. Inter-Laminar Shear Strength by Double-Notch Shear Test

In this section, quasi-static and high-strain-rate tests on DNS specimens mentioned in the previous section are discussed. The standard ASTM D 3846 recommends loading the DNS specimen in tension for quasi-static loading. However, this is not feasible in the case of high-strain-rate experiments, and hence, the samples were loaded in compression in both quasi-static and high-strain-rate tests. For high-strain-rate loading, a split Hopkinson pressure bar (SHPB) having 20-mm-diameter incident and transmitter bars made of Vascomax 300 steel was used.

Two DNS specimens were tested at a crosshead rate of 0.5 mm/min. Figure 2(a) shows the typical signals from quasi-static tests. In high-strain-rate tests, four DNS specimens were tested. Figure 2(c) shows the typical incident (ϵ_i) and reflected (ϵ_r) signals from a high-strain-rate test. The transmitted force, $F(t)$ and the shear stress, $\tau(t)$ in the specimen were calculated as follows.

$$F(t) = A_b E_b (\epsilon_i + \epsilon_r) \text{ and}$$
$$\tau(t) = 0.75 \frac{F(t)}{W * T}, \qquad \text{(Eq 1)}$$

where A_b and E_b are, respectively, the area of cross section and the Young's modulus of the bar, and W and T are the width and thickness (depth) of the specimen, respectively, assuming the load to be shared equally between the two inter-laminar planes. The stress–time history for this test is shown in Fig. 2(d). The shear strain distribution in the specimen, measured using DIC
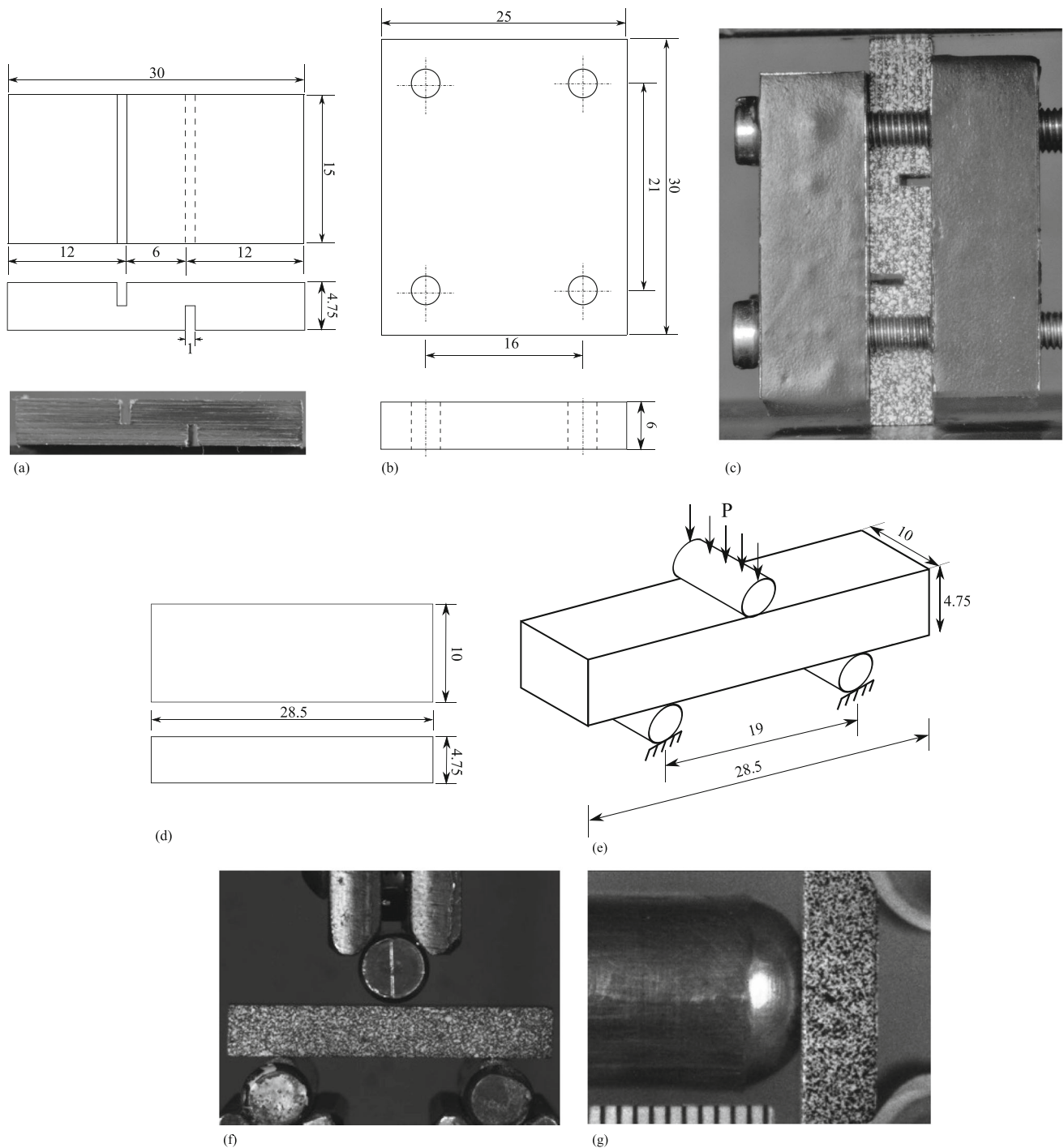
Fig. 1 (a) Details of DNS specimen with photograph. (b) Loading jig for DNS specimen. (c) Photograph of DNS specimen held in the loading jig. (d) An SBS specimen. (e) Loading arrangement for SBS specimen. SBS specimens in (f) quasi-static loading and (g) high-strain-rate tests. All dimensions are measured in *mm*

in a quasi-static and high-strain-rate test, is shown in Fig. 2(b) and (e), respectively. In the quasi-static test, the shear strain at failure is 3.36%, while for the high-strain-rate test, the failure strain is 1.5%. The strain in the failed section is reasonably homogeneous. The images of the specimens after the test are shown in Fig. 2(f). It can be observed that failure is mostly inter-laminar connecting the two notch tips.

4. Inter-Laminar Shear Strength by Short Beam Shear Test

ILSS tests were performed using the short beam shear specimen with geometry as mentioned in ASTM D2344 and as described in Fig. 1(d). The loading configuration was devised for tests as shown in Fig. 1(e), and a random speckle pattern was applied on the specimen to enable displacement and strain
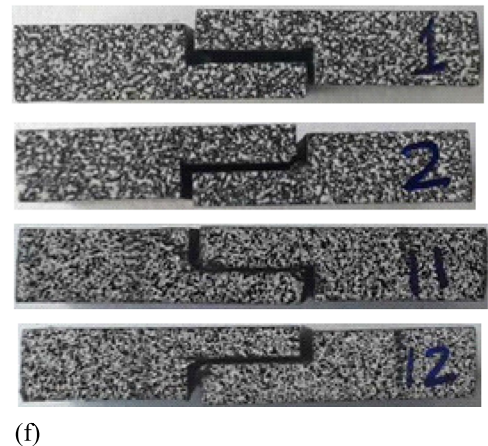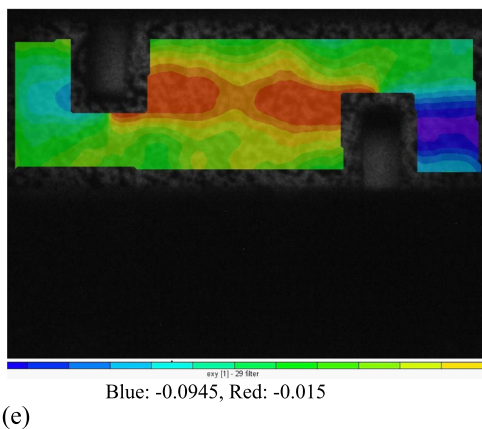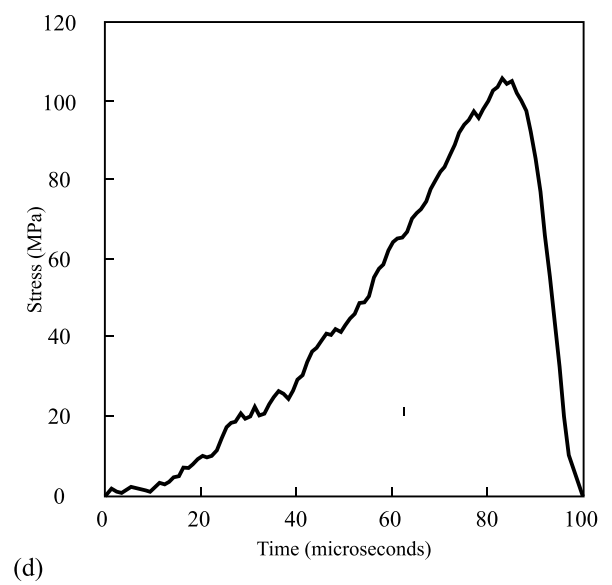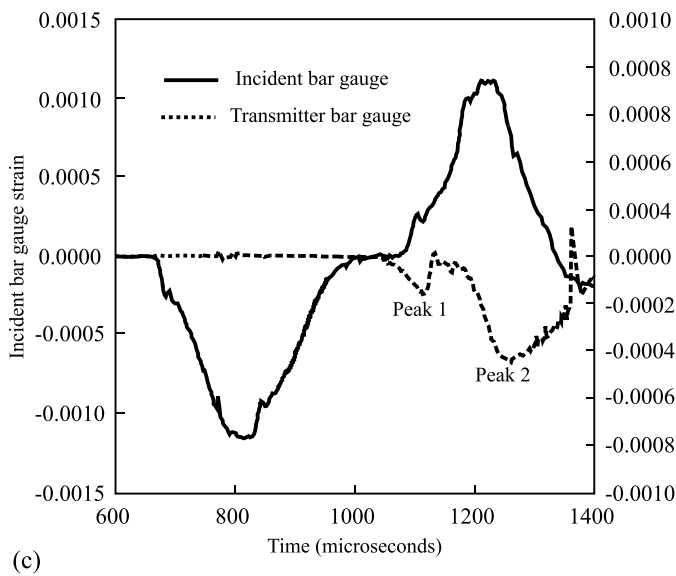
(a)

(b)

Blue: -0.034, Red: 0.008

(c)

(d)

(e)
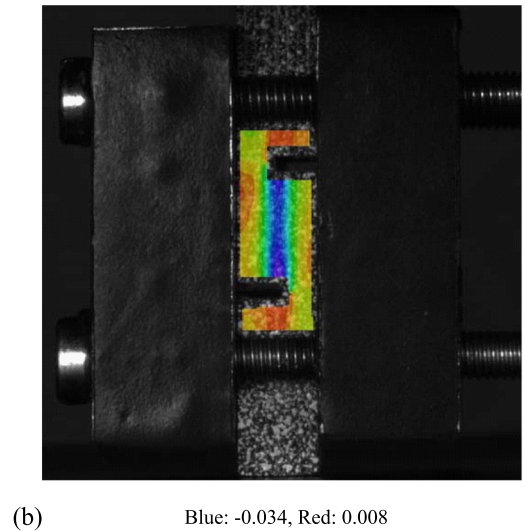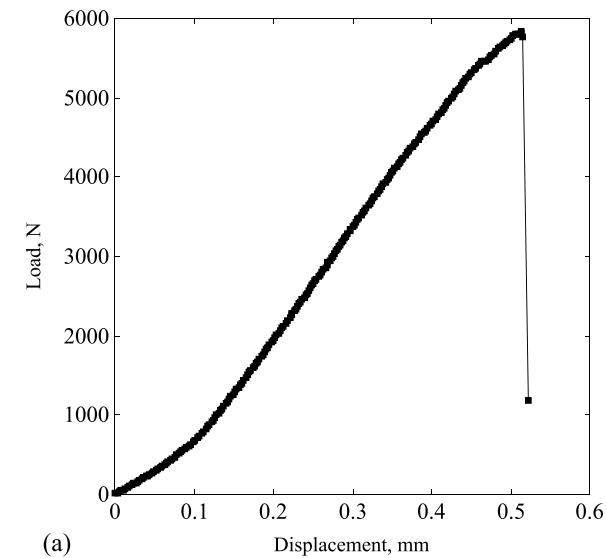
Blue: -0.0945, Red: -0.015

(f)

Fig. 2 (a) Typical load–displacement behavior and (b) shear strain distribution in the DNS specimen just prior to failure in quasi-static test. (c) Strain signals and (d) stress–time history in the specimen for the strain records shown in (c). (e) Shear strain distribution in the specimen just prior to failure in a high-strain-rate test. (f) Photographs of the specimens after failure

measurements using DIC. The specimens and loading configurations for quasi-static and high-strain-rate tests are shown in Fig. 1(f) and (g). The quasi-static tests were conducted on two SBS specimens using a UTM at a crosshead rate of 0.5 mm/minute. The high-strain-rate tests were performed using an SHPB having a 12.6-mm-diameter incident bar made of aluminum.

A typical load–displacement curve obtained in the quasi-static test is shown in Fig. 3(a). In high-strain-rate tests, four SBS specimens were tested. Figure 3(c) shows a typical incident (ϵ_i) and reflected (ϵ_r) signals from a high-strain-rate test. The transmitted force and the shear stress in the specimen were calculated using Eq. 1 as mentioned earlier. The shear strain distribution in the specimen is shown in Fig. 3(b) and (d) in quasi-static and high strain rate, respectively. The shear strain at failure is 1.9% in quasi-static loading and 4.2% in high-strain-rate loading. The strain in the failed section is homogeneous in case of SBS, as well.

5. SEM Fractography on Tested Specimens

At the outset, the microstructure of the composite layup was observed under scanning electron microscope (SEM) to see the fiber distribution and fiber–matrix interface as shown in Fig. 4(a). The images were obtained from a field emission scanning electron microscope (Sigma, Zeiss, Germany). The microstructure of the sample can be observed with ply interfaces. Barile et al. (Ref 19) have observed that the homogeneous microstructures result in improved ILSS of the specimens. The SEM images of the tested DNS specimen reveal intra-layer microcracking (Fig. 4b), large delamination (Fig. 4c) and inter-laminar de-bonding (Fig. 4d). The phenomenon of microcracking appears to be continued along the ply interface causing inter-laminar propagation. The SEM images of the tested SBS specimen shown in Fig. 4(e)-(f) reveal the fact that the flexural failure is the dominant mode over the breaking of the specimen. Few more damage modes in SBS specimens are shown in Fig. 4(g)-(i).

6. Results and Discussion

In spite of inter-laminar failure in all DNS specimens, a scatter in the strength is observed. The scatter is inherent due to the variance in the depth of the two notches. The notch depth should be exactly half of the specimen thickness which was difficult to achieve with tight tolerance using the machine facility available in-house. From the stress–time history and the real-time images of failure in a typical test (as shown in Fig. 2(d) and Fig. 5), it can be observed that the specimen reaches its maximum stress slightly after 80 microseconds. The time instants marked in Fig. 5 correspond to the time given in the stress history shown in Fig. 2(d). After 80 microseconds, the stress drops suddenly due to specimen failure. The loading rate in this test is obtained as 1.96 MPa/μs.

The image corresponding to 90 microseconds in Fig. 5 shows failure in the specimen. This confirms that the failure of the specimen occurs at the first peak in the transmitted signal shown in Fig. 2(c). After failure, the specimen halves, slides and comes into contact at the notch surfaces and starts transferring further load resulting in the second peak in the transmitted signal. Overall, the results indicate that there is an increase in the strength from quasi-static to high strain rate.

Real-time images of failure in a typical SBS test are shown in Fig. 3(e). For the specimens tested in high-strain-rate loading, a stress–time history is calculated and plotted as shown in Fig. 6(a)-(d). Moreover, a time history for one of the specimens is re-plotted with marking of two time events to highlight the specimen just prior and after the failure, as shown in Fig. 6(e). The discontinuity in the displacement is also shown in the insets (Fig. 6f) which correspond to two images before and after specimen failure. There is drop in load after failure, which can be observed from stress history (Fig. 6e).

The specimen reaches its maximum stress slightly after 100 microseconds, and then, the stress drops suddenly due to specimen failure. The loading rate in this test is calculated as 2.04 MPa/μs. From the images of the specimens after the test as shown in Fig. 7, it can be observed that failure is mostly inter-laminar and the failure has taken place in one half of the specimen. This might have happened because of asymmetric load with respect to specimen length. The results indicate that there is an increase in the strength from quasi-static to high strain rate in the SBS test, as well.

Moreover, the inter-laminar shear strength is remarkably strain rate dependent and there is an increase in the inter-laminar shear strength by 32% in DNS and 90% in SBS, from quasi-static to high-strain-rate load. The phenomena of the increase in the relative ILSS with strain rate is apparently an effect of fiber weight fraction. Hence, it is difficult to get a simple explanation based on the present work. Further experimental work with a set of controlled parameters is needed to further insights.

The work accomplished in this manuscript may improve the understanding of inter-laminar shear behavior of the adhesion in carbon fiber/matrix. The two approaches of investigation, namely quasi-static and high strain rate, may benefit the reader in selecting the loading rate suitable for the application under consideration. This manuscript has presented both the techniques with modern tools of data collection and processing with deliverables of reliable estimates of the strength.

7. Conclusions

The inter-laminar shear performance of a carbon fiber-reinforced composite was studied with the help of experimental techniques using two distinct specimens and loading configurations. In the double-notch shear specimen, the interface was directly subjected to shear load, while in the short beam shear specimen, the interface was loaded in flexure. Both the approaches delivered fairly homologous results with some scatter in the magnitude of shear strength. The lack of exactness in notch depth in double-notch shear tests was observed to be the cause of scattered results. In short beam shear tests, on the other hand, it was observed that load might not be symmetrically applied with respect to specimen length.

In the double-notch shear test, the shear strain at failure is 3.36% under quasi-static load, while for the high-strain-rate test the failure strain is 1.5%. The average inter-laminar shear strength is found to be 69.8 MPa under quasi-static load and 92.25 MPa under high-strain-rate loading. In the short beam shear test, on the other hand, the shear strain at failure is found
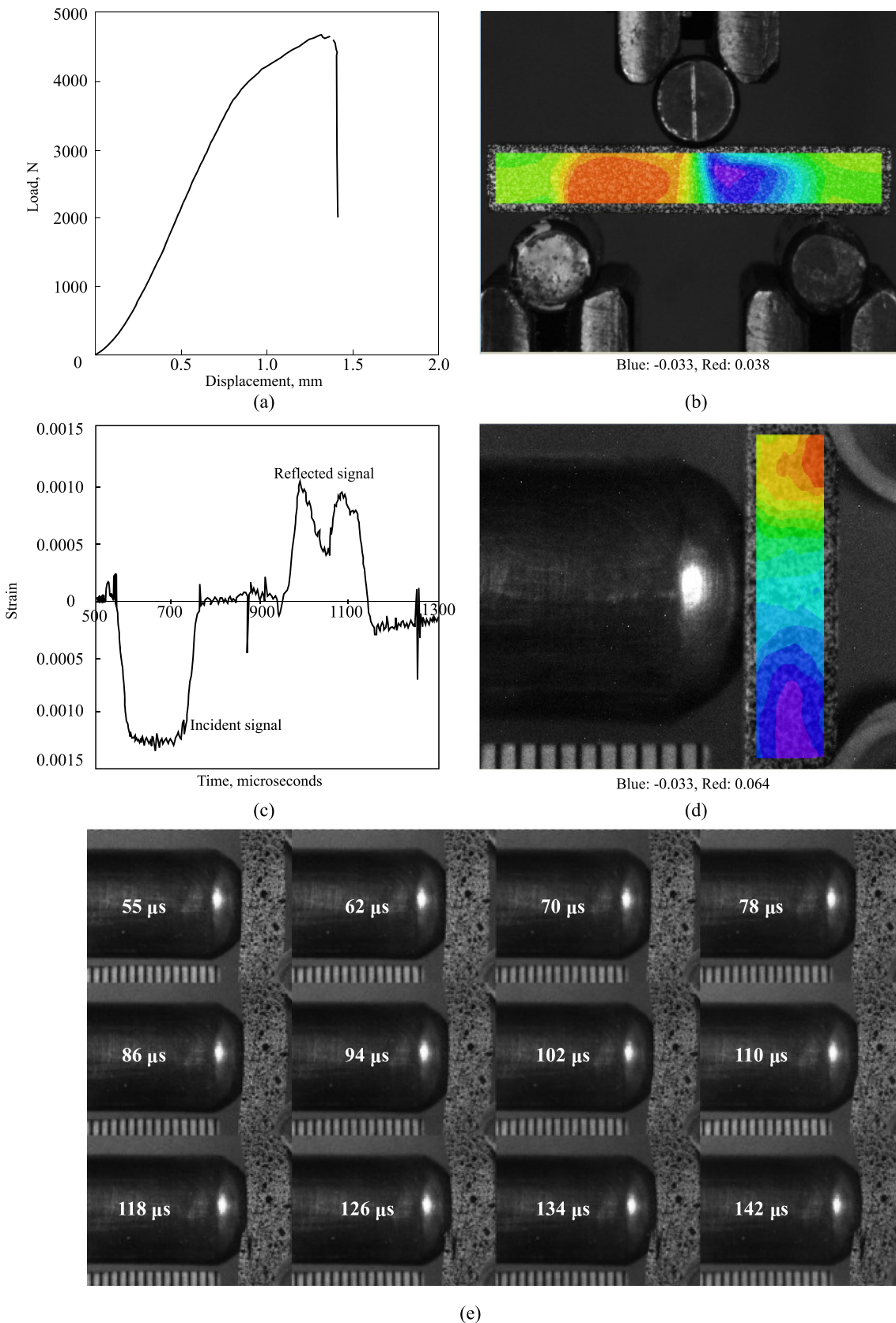
Fig. 3 (a) Typical load–displacement behavior and (b) shear strain distribution in the SBS specimen in quasi-static test. (c) Strain signals and (d) shear strain distribution obtained in the SBS specimen in a high-strain-rate test. (e) Real-time images of the specimen during the test
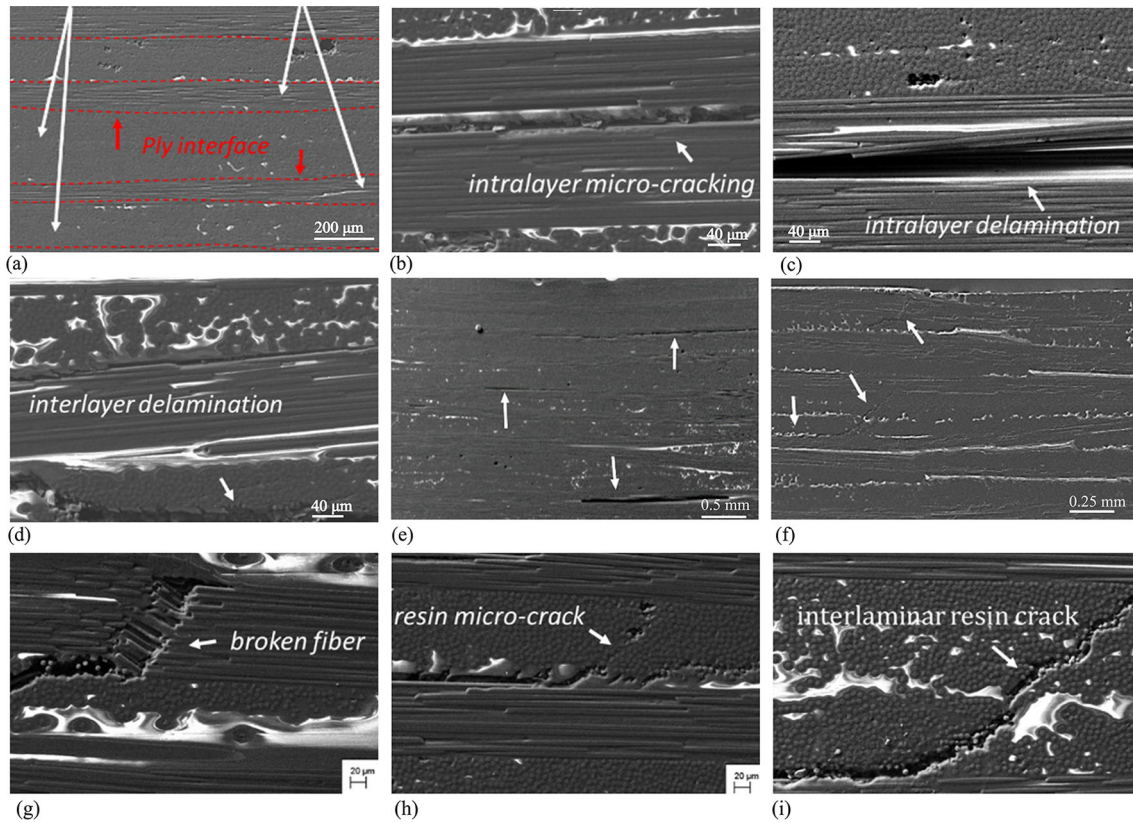
Fig. 4 (a) Fiber layup in the specimens indicating the interfaces. SEM images of the DNS specimen with indication of (b) intra-layer microcracking, (c) inter-layer delamination and (d) large delamination between the fibers in the shear plane. The damage evolution in the SBS specimens after the test is shown in (e, f). SEM images of the SBS specimen showing various failure modes: (g) fiber fracture, (h) microcracks and (i) inter-laminar cracks
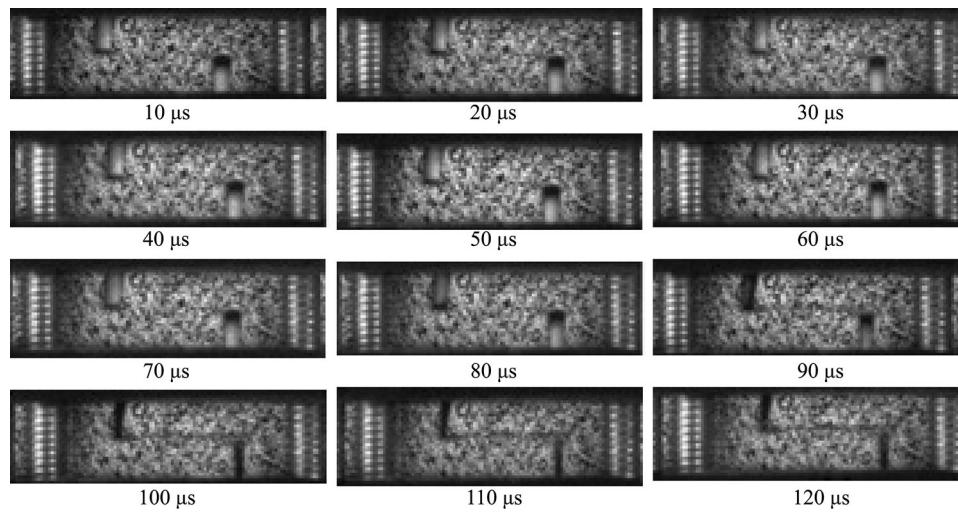

Fig. 5 Real-time images of failure of DNS specimen in high-strain-rate test

to be 1.9% under quasi-static load, while for the high-strain-rate test the failure strain is 4.2%. The average inter-laminar shear strength of the composite layup is measured to be about 73.9 MPa and 140.7 MPa, respectively, under quasi-static and high-strain-rate loading.

Overall, it is observed that failure is mostly inter-laminar and the results suggest that inter-laminar shear strength is strain rate dependent with a remarkable increase from quasi-static to high strain rate. Further experimental work with a careful
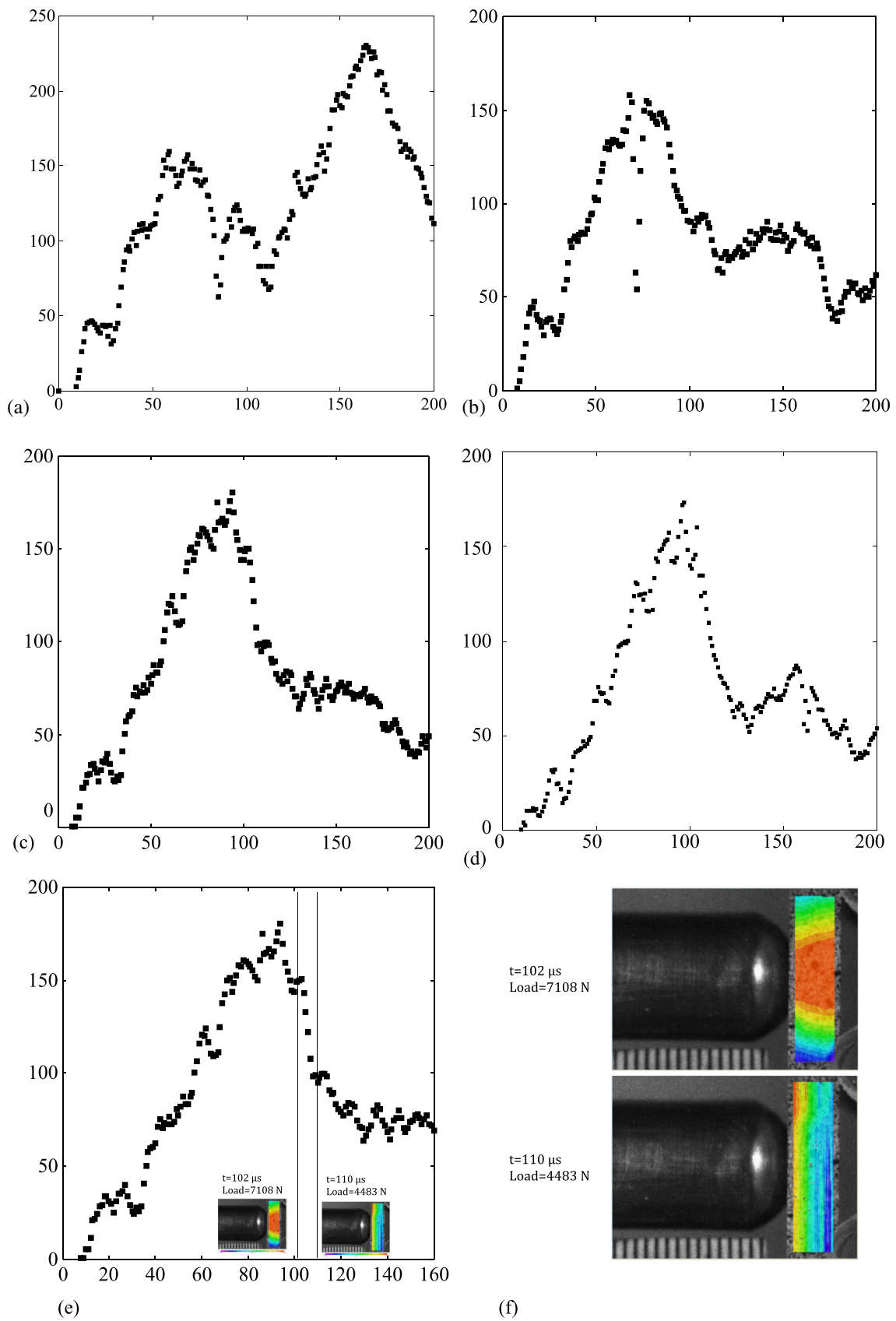
Fig. 6 (a)-(d): Stress–time history for high-strain-rate specimens D3, D4, D6 and D7, respectively. (e) Time history for D6 specimen with marking of two time events just prior and after the failure. (f) Discontinuity in the displacement in D6 specimen just prior and after the failure
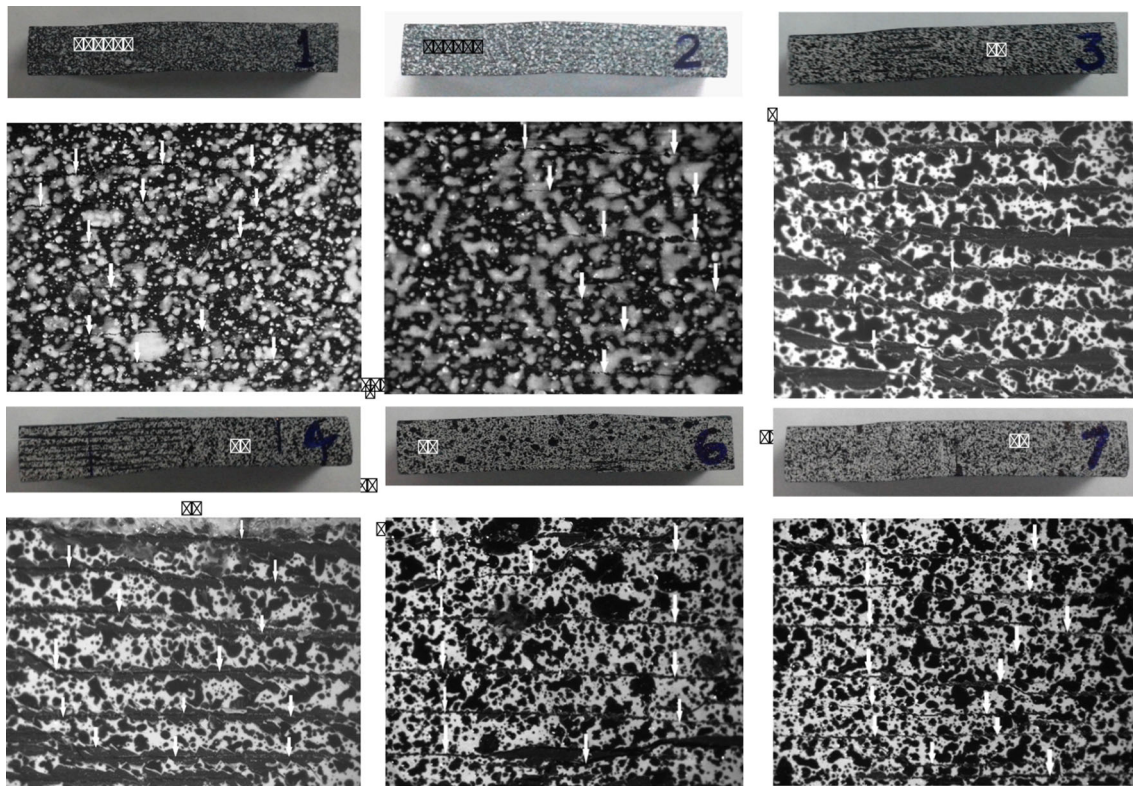
Fig. 7 Real-time images of failure of SBS specimen in high-strain-rate test

control of the various parameters involved is required to get a plausible answer.

Funding

This research did not receive any specific grant from funding agencies in the public, commercial, or not-for-profit sectors.

Conflict of interest

None.

References

1. X. Chen, H. Xu, D. Liu, C. Yan, and Y. Zhu, A Facile One-pot Fabrication of Polyphosphazene Microsphere/carbon Fiber Hybrid Reinforcement and its Effect on the Interfacial Adhesion of Epoxy Composites. Appl. Surf. Sci. **410**, 530–539 (2017). (**ISSN 0169-4332**)
2. S.-S. Yao, F.-L. Jin, K.Y. Rhee, D. Hui, and S.-J. Park, Recent Advances in Carbon-Fiber-Reinforced Thermoplastic Composites: A Review. Compos. B Eng. **142**, 241–250 (2018). (**ISSN 1359-8368**)
3. F. Yan, L. Liu, K. Li, L. Jin, M. Zhang, Y. Liu, L. Xiao, and Y. Ao, A Novel p Bridging Method to Graft Graphene Oxide onto Carbon Fiber for Interfacial Enhancement of Epoxy Composites. Compos. Sci. Technol. **201**, 108489 (2021). (**ISSN 0266-3538**)
4. S. Li, D. Chen, Y. Yuan, C. Gao, Y. Cui, H. Wang, X. Liu, M. Liu, and Z. Wu, Influence of Flexible Molecular Structure on the Cryogenic Mechanical Properties of Epoxy Matrix and Ccarbon Fiber/Epoxy Composite Laminate. Mater. Design **195**, 109028 (2020). (**ISSN 0264-1275**)
5. E.A. Hassan, D. Ge, S. Zhu, L. Yang, J. Zhou, and M. Yu, Enhancing CF/PEEK Composites by CF Decoration with Polyimide and Loosely-Packed CNT Arrays. Compos. A Appl. Sci. Manuf. **127**, 105613 (2019). (**ISSN 1359-835X**)
6. Y. Wu, Z. Wang, L. Xu, H. Wang, S. Peng, L. Zheng, Z. Yang, L. Wu, and J.-T. Miao, Preparation of Silver-Plated Carbon Nanotubes/Carbon Fiber Hybrid Fibers by Combining Freeze-Drying Deposition with a Sizing Process to Enhance the Mechanical Properties of Carbon Fiber Composites. Compos. A Appl. Sci. Manuf. **146**, 106421 (2021). (**ISSN 1359-835X**)
7. E.A. Hassan, L. Yang, T.H. Elagib, D. Ge, X. Lv, J. Zhou, M. Yu, and S. Zhu, Synergistic Effect of Hydrogen Bonding and p-p Stacking in Interface of CF/PEEK Composites. Compos. B Eng. **171**, 70–77 (2019). (**ISSN 1359-8368**)
8. Y.S. Kim, U. Jung, S. Choi, Y.C. Jung, H.-S. Lee, and J. Kim. Effect of Plasma Gas and Ar Incorporation on the Shear Strength Between Carbon Fiber-Reinforced Thermoplastic Polymer and Al. Compos. A Appl. Sci. Manuf. **138**, 106041 (2020). (**ISSN 1359-835X**)
9. S.S. Chee, M. Jawaid, M. Sultan, O.Y. Alothman, and L.C. Abdullah, Accelerated Weathering and Soil Burial Effects on Colour, Biodegradability and Thermal Properties of Bamboo/Kenaf/Epoxy Hybrid Composites. Polym. Testing **79**, 106054 (2019). (**ISSN 0142-9418**)
10. M. Sultan, K. Worden, W. Staszewski, and A. Hodzic, Impact Damage Characterisation of Composite Laminates Using a Statistical Approach. Compos. Sci. Technol. **72**(10), 1108–1120 (2012). **ISSN 0266-3538**
11. M. Suriani, R. Ilyas, M. Zuhri, A. Khalina, M. Sultan, S. Sapuan, C. Ruzaidi, F.N. Wan, F. Zulkifli, and M. Harussani, et al., Critical Review of Natural Fiber Reinforced Hybrid Composites: Processing, Properties, Applications and Cost. Polymers **13**(20), 3514 (2021)
12. J. Naveen, M. Jawaid, E. Zainudin, M. Sultan, and R. Yahaya, Mechanical and Moisture Diffusion Behaviour of Hybrid Kevlar/*Cocos nucifera* Sheath Reinforced Epoxy Composites. J. Market. Res. **8**(1), 1308–1318 (2019)
13. K. Balasubramanian, M.T. Sultan, and N. Rajeswari, Manufacturing Techniques of Composites for Aerospace Applications, in: Sustainable Composites for Aerospace Applications, Elsevier, 55–67 (2018)
14. F. Mustapha, K. Aris, N. Wardi, M. Sultan, and A. Shahrjerdi, Structural Health Monitoring (SHM) for Composite Structure Undergoing Tensile and Thermal Testing. J. Vibroeng. **14**(3), 1342–1353 (2012)

15. M. Sayyad, V. Parameswaran, and S. Basu. Stiffness and Toughness Gradation of Bamboo from a Damage Tolerance Perspective. Int. J. Solids Struct. **143**, 274–286 (2018)

16. J. Ma, L. Jiang, Y. Dan, and Y. Huang, Study on the Inter-Laminar Shear properties of Carbon Fiber Reinforced Epoxy Composite Materials with Different Interface Structures. Mater. Design. **214**, 110417 (2022). (**ISSN 0264-1275**)

17. M. Zhang and S. Mason, Interlaminar Shear Strength of Carbon Fibre Reinforced Epoxy Composite Under the Influence of Environments. Adv. Compos. Lett. **7**(1), 096369359800700104 (1998)

18. S. Uvarov and V. Chudinov, Dynamic and Quasistatic Interlaminar Shear Strength of Carbon Fiber Laminate Under Bi-axial loading Conditions. In: 26th International Conference on Fracture and Structural Integrity, Procedia Structural Integrity **33**, 465–468 (2021). **ISSN 2452-3216**

19. C. Barile, C. Casavola, G. Pappalettera, V.P. Kannan, and G. Renna, Investigation of Interlaminar Shear Properties of CFRP Composites at Elevated Temperatures Using the Lempel-Ziv Complexity of Acoustic Emission Signals. Materials **15**(12), 4252 (2022)